Optical Thomson Scattering

D. H. Froula, J. P. Palastro, and R. K. Follett

Laboratory for Laser Energetics, University of Rochester

Introduction

Thomson scattering provides a direct observation of electron motion in a plasma by encoding their velocities on the frequency spectrum of the scattered light. By propagating a beam of photons (ω_0, $\mathbf{k}_0$) through a plasma and isolating the Thomson-scattering volume collected into a spectrometer (Fig. 1), a spatially resolved measurement of the plasma conditions can be determined from the scattered frequency spectrum (ω_s, $\mathbf{k}_s$) (Ref. 1). The scattered-power spectrum observed by the detector is given by

$$\frac{\mathrm{d}P_s}{\mathrm{d}\omega_s} = \frac{P_i r_0^2 L \mathrm{d}\Omega}{2\pi}\left(1+\frac{2\omega}{\omega_0}\right) n_e S(\mathbf{k},\omega), \tag{1}$$

where $r_0^2 = 7.95\times10^{-26}$ cm is the classical electron radius, L is the length of the scattering volume along the probe beam, $\mathbf{k} = \mathbf{k}_s - \mathbf{k}_0$, $\omega = \omega_s - \omega_0$, $\mathrm{d}\Omega$ is the solid angle of the collected scattered photons, and P_i is the average incident laser power. The density fluctuations of the plasma around its average density dictate the primary shape of the scattered spectrum through the dynamic structure factor. For a collisionless plasma with no magnetic fields affecting the motion of the particles, the dynamic structure factor is

$$S(\mathbf{k},\omega) = \frac{2\pi}{k}\left|1-\frac{\chi_e}{\varepsilon}\right|^2 f_e\left(\frac{\omega}{k}\right) + \sum_j \frac{2\pi}{k}\frac{Z_j^2 n_j}{n_e}\left|\frac{\chi_e}{\varepsilon}\right|^2 f_j\left(\frac{\omega}{k}\right), \tag{2}$$

where f_e and f_j are the normalized 1-D electron and ion-velocity distribution functions, respectively, projected along the scattering vector ($\mathbf{k}$), Z_j is the average charge of the jth ion species, $n_e = \sum_j n_j Z_j$, and n_j is the density of jth ion species. The longitudinal dielectric function is

$$\varepsilon = 1 + \chi_e + \sum_j \chi_j, \tag{3}$$

where the kinetic plasma susceptibilities are given by

$$\chi_e(\mathbf{k},\omega) = \frac{4\pi e^2 n_e}{m_e k^2}\int_{-\infty}^{\infty} \mathrm{d}\mathbf{v}\frac{\mathbf{k}\cdot\partial f_e/\partial \mathbf{v}}{\omega - \mathbf{k}\cdot\mathbf{v}}, \tag{4}$$

$$\chi_j(\mathbf{k},\omega) = \frac{4\pi Z_j^2 e^2 n_j}{m_j k^2}\int_{-\infty}^{\infty} \mathrm{d}\mathbf{v}\frac{\mathbf{k}\cdot\partial f_i/\partial \mathbf{v}}{\omega - \mathbf{k}\cdot\mathbf{v}}, \tag{5}$$

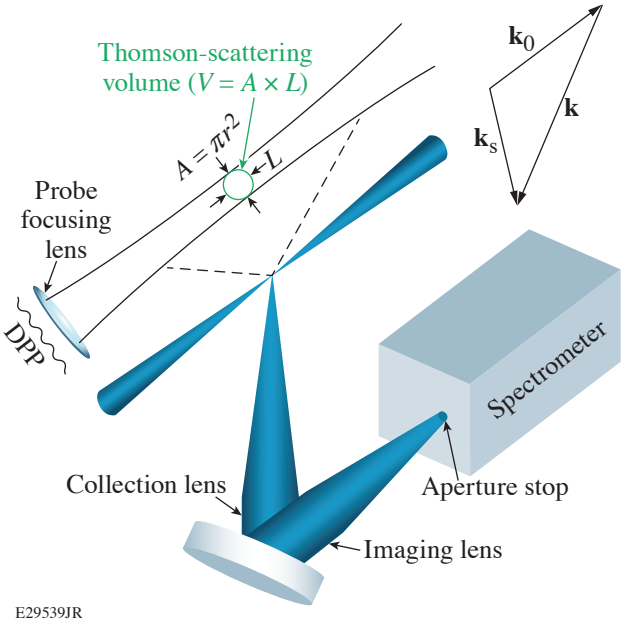

Figure 1
A typical Thomson-scattering system is shown where the probe laser beam propagates through a distributed phase plate (DPP) before being focused to an area (A) at the Thomson-scattering volume. An aperture stop is imaged into the plasma to define the Thomson-scattering volume along the propagation of the probe beam (L).

The scattering spectrum can be used to measure the electron distribution function, which is most evident in the high-frequency noncollective Thomson-scattering regime. Here the collective motion of the electrons is heavily damped and the power scattered at a particular frequency is proportional to the number of electrons with a velocity that Doppler shifts the frequency of the probe laser to the measured frequency [Fig. 2(a)]. In this strong damping regime, where the scattering parameter $\alpha \equiv 1/k\lambda_{De} \ll 1$ ($\lambda_{De}^2 = \kappa T_e/4\pi e^2 n_e$ is the electron Debye length), Eq. (1) is reduced to light that is scattered from an ensemble of uncorrelated electrons,

$$\frac{dP_s}{d\omega_s} = \frac{P_i r_0^2 L d\Omega}{2\pi}\left(1 + \frac{2\omega}{\omega_0}\right) n_e f_e(\omega/k). \tag{6}$$

From here it is evident that the noncollective spectrum provides a direct measurement of the electron distribution function, but in practice, the small scattering cross section of the electron and the small number of electrons at high velocities lead to low signal-to-noise, typically limiting this technique to measuring electrons in the bulk of the distribution function.

It is also possible to measure the electron distribution function in the regime where the high-frequency scattering spectrum is governed by the collective electron motion introduced by weaker damping of the density fluctuations.[2,3] In this collective regime, the thermal particle motion drives a rich spectrum of fluctuations, which when probed, can present themselves in the scattering spectrum as peaks shifted around the incident frequency of the laser (Fig. 2). As charged particles propagate through the plasma, they leave electrostatic fluctuations in their wake. The amplitude of each fluctuation is determined by the balance of its damping rate with the rate at which it is driven by the plasma particles. The high-frequency electron plasma wave fluctuations start to play an important role in the scattering spectrum when $\alpha \sim 2$, but when the fluctuations are more weakly damped ($\alpha \geqslant 2$), the resonant features have separated clearly from the noncollective scattering spectrum [Fig. 2(a)]. For the low-frequency fluctuations [Fig. 2(b)], there are similar regimes, but related to the ion motion. The transition between the collective and noncollective regime in a collisionless plasma is governed by the ion Landau damping, and the collective low-frequency regimes occur for the scattering parameter $\alpha > \left(ZT_e/3T_i - 1\right)^{-1/2}$. For $ZT_e/3T_i < 3$, the fluctuations are heavily damped by the ions.

The frequency of these resonant peaks can be found approximately by solving the dispersion relation ($\varepsilon = 0$) for the natural modes of the plasma by finding the real parts of the roots of the dielectric function [Eq. (3)], which is where one can see the power of collective Thomson scattering in determining the plasma conditions. Assuming Maxwellian electron distribution functions and weakly

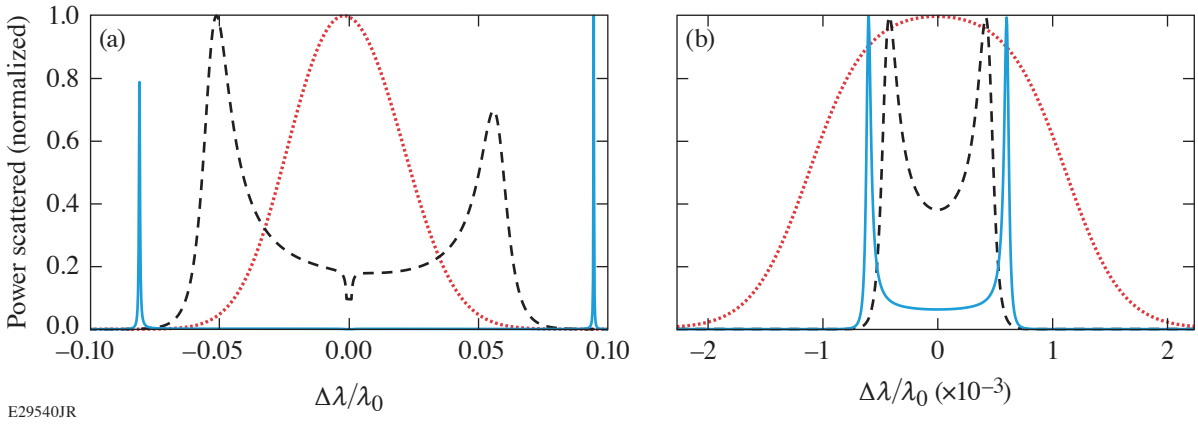

Figure 2
(a) High-frequency spectrum calculated from Eq. (1) in the heavily damped noncollective regime, $\alpha = 0.25$ (red dotted curve); mildly damped collective regime, $\alpha = 2.0$ (black dashed curve); and weakly damped collective regime, $\alpha = 4.0$ (blue solid curve). The temperature was maintained at $T_e = 100$ eV and the density was scaled $n_e = 1 \times 10^{17}$ cm^{-3} (red), $n_e = 6 \times 10^{18}$ cm^{-3} (black), $n_e = 2.5 \times 10^{19}$ cm^{-3} (blue). The low-frequency spectrum has been suppressed. (b) The low-frequency spectrum calculated from Eq. (1) in the heavily damped noncollective regime, $ZT_e/T_i = 0.5$ (red); mildly damped collective regime $ZT_e/T_i = 3.5$ (black); and weakly damped collective regime $ZT_e/T_i = 10$ (blue). The scattering parameters $\alpha = 2$ and $T_e/T_i = 10$ were held constant. For all calculations, the angle between incident and scattered light was held constant ($\theta = 90°$).

damped fluctuations, the real part of the dispersion relation for the ion-acoustic waves simplifies to $\omega_{iaw} \simeq k\sqrt{\left[\left(Z\kappa T_e + 3\kappa T_i\right)/m_i\right]}$, in the low-frequency spectrum, and the real part of the high-frequency part of the dispersion relation, corresponding to the electron plasma waves simplifies to $\omega_{epw}^2 = \omega_{pe}^2 + 3\kappa T_e k^2/m_e$, where $\omega_{pe}^2 = 4\pi n_e e^2/m_e$ is the electron plasma frequency. Thomson-scattered light from these collective electron motions generates constructive interference at the detector plane, and the frequency of this interference can be directly related to the plasma conditions through the plasma dispersion relations; note that measuring the difference between the frequency of the laser and the peak features in the spectrum ($\omega = \omega_s - \omega_0 = \Delta\omega$) is a measure of the plasma conditions through the associated dispersion relations ($\Delta\omega/\omega_0 \approx \Delta\lambda/\lambda_0$).

Collective Thomson scattering is a powerful diagnostic regime used to overcome background radiation because of the need to resolve only the frequencies of the spectral peaks. This is in contrast with the noncollective regime, where the shape of the scattering spectrum is used to infer the plasma conditions, therefore challenging one to understand the background radiation spectrum and the wavelength sensitivity of the diagnostic. In practice, modern collective Thomson-scattering systems can resolve the complete spectrum, providing detailed measurements of the electron distribution functions,[4] electron temperatures, ion temperatures,[5,6] plasma flow velocities, and electron densities.[7,8]

Laser Beam Propagation

The small Thomson-scattering cross section is one of the most-challenging aspects of Thomson scattering. Integrating Eq. (1) over frequency provides the total power scattered, $P_s/P_i \simeq (8\pi/3) n_e r_0^2 L d\Omega \sim 10^{-12}$ for typical parameters ($n_e = 10^{19}$ cm^{-3}, $L = 50$ μm, $d\Omega = 10^{-4}$). To overcome this small cross section, lasers are used to deliver sufficient power to the Thomson-scattering volume, but the laser power must be balanced against laser–plasma instabilities that can prevent the laser beam from reaching the Thomson-scattering volume. One of the most-limiting instabilities is ponderomotively driven self-focusing. For a laser beam with a Gaussian spatial profile, the self-focusing power threshold is $P_c = 3 \times 10^7 \left[T_e(\text{keV})/n_e/n_c\right]$, where $n_c = m_e \omega_0^2/4\pi e^2$ is the critical density for the probe laser.

By limiting the power of the laser to the critical power for self-focusing, the maximum power scattered is given by

$$P_s^{max}(\text{W}) \simeq 4 \times 10^{-29} \omega_0^2 T_e(\text{eV}) L(\text{cm}) d\Omega. \quad (7)$$

To demonstrate how restrictive this condition is on the parameter space accessible by Thomson scattering, the signal-to-noise can be calculated by assuming Poison statistics, $S/N \approx \sqrt{P_s^{max}\,\Delta t/\hbar\omega_0}$, where $\hbar$ is Planck's constant.[9] For typical conditions (T_e = 100 eV, $L = 10^{-2}$ cm, $d\Omega = 10^{-4}$, $\omega_0 = 3.8 \times 10^{15}$ 1/s), spread evenly over 100 resolution units in an ideal system suggests $S/N \sim 10$. From here, it is evident that Thomson scattering requires high electron temperatures, long integration times (Δt), large Thomson-scattering volumes along the axis of the probe beam (L), or large solid angle collection optics ($d\Omega$) to increase the signal-to-noise, but each of these parameters has significant constraints within the experimental design.

Intuitively one would expect higher laser powers or higher densities to improve the signal-to-noise, but once the laser power has reached the critical power for self-focusing, the beam will not propagate well to the Thomson-scattering volume. Increasing the density does not help because the increased signal that results from the higher density is directly compensated by the need to reduce the laser power to remain below the critical power for self-focusing. One way to overcome self-focusing, typically at the cost of increasing the Thomson-scattering volume, is to use a DPP.[10] A DPP introduces spatial phase modulation across the laser beam prior to the focusing lens. This phase increases the diameter of the laser spot by distributing the laser power into many speckles, which increases the self-focusing threshold by a factor of ~100 (Ref. 9).

Thomson Scattering from a Maxwellian Plasma

Figure 2 shows the high-frequency and low-frequency parts of the Thomson-scattering spectrum calculated using Eq. (1) assuming Maxwellian ion and electron distribution functions. To measure these spectra, a typical Thomson-scattering instrument uses two spectrometers to independently resolve the high-frequency and low-frequency regimes.[11,12] The high-frequency spectrum requires lower dispersion to spread the $\Delta\lambda/\lambda_0 \sim 0.1$ spectrum over a detector with approximately 200 resolution units. This can be achieved with a 1/3-m spectrometer with a 150-grooves/mm grating. Resolving the low-frequency spectrum requires a high-dispersion system that can resolve the separation between the ion-acoustic peaks $\Delta\Lambda/\lambda_0 \sim 10^{-3}$ over at least 20 resolution units. This can be achieved with a 1-m spectrometer with a 2400-grooves/mm grating. Often the spectrometers are coupled to optical streak cameras to measure the evolution of the plasma conditions. In these systems, the temporal resolution is determined by the pulse-front tilt introduced by the spectrometers, which is typically of the order of 100 ps (Ref. 13). By trading unrealized spectral resolution for improved time resolution, the temporal resolution can be optimized to the Heisenberg limit.[14,15]

1. High-Frequency Fluctuations—Electron Plasma Waves

Figure 3 shows the sensitivity of the high-frequency spectrum to the plasma conditions in three different scattering regimes. In the weakly damped regime, the scattering features are very narrow and the sensitivity of the frequency of their peaks provides an accurate measure of the electron density. In this regime, the width of these features is typically dominated by instrument

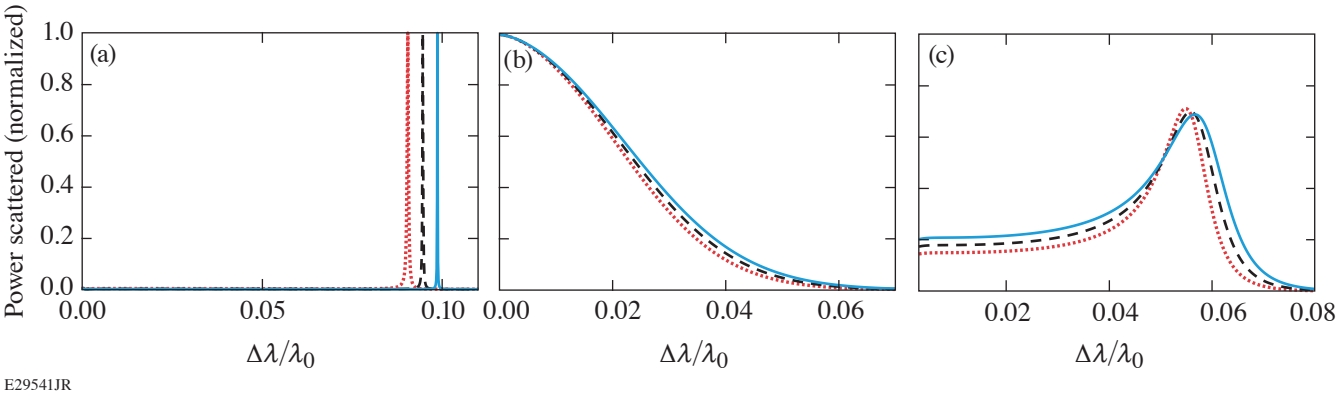

Figure 3
The sensitivity of the spectrum shown in Fig. 2 to (a) the electron density in the weakly damped regime and electron temperature in (b) the strongly damped regime and (c) the mildly damped regime. The parameters were varied around the central value (black) by +10% (blue) and –10% (red).

broadening and density gradients within the Thomson-scattering volume.[16] By reducing the scattering parameter such that the waves are mildly damped, their width can be increased significantly beyond typical broadening due to gradients and the shape becomes an accurate measurement of the electron temperature, while the peak location remains a measure of the electron density. Further increasing the damping results in a noncollective spectrum where the shape of the scattering spectrum represents the electron distribution function.

2. Low-Frequency Fluctuations—Ion-Acoustic Waves

Figure 4(a) shows the sensitivity of the low-frequency spectrum in the collective regime to the product ZT_e. In this weakly damped regime, the scattering features are very narrow and the sensitivity of their peak location in frequency provides an accurate measure of ZT_e, provided $ZT_e \gg 3T_i$. When this condition is not met, it is convenient to work in the mildly collective regime, where the shape of the ion-acoustic peaks can be resolved, providing a measure of the ion temperature [Fig. 4(b)]. Another technique that is often used to measure the ion temperature in low-Z plasmas is to introduce a small fraction of higher-Z atoms.[5,6] When the ratio of atomic number to the average ionization (A/Z) is sufficiently different between the two species, additional low-frequency modes are resolvable in the scattering spectrum [Fig. 4(c)].[17] From the relative amplitudes of these two modes, an accurate measure of the ion temperature can be obtained.[8,18]

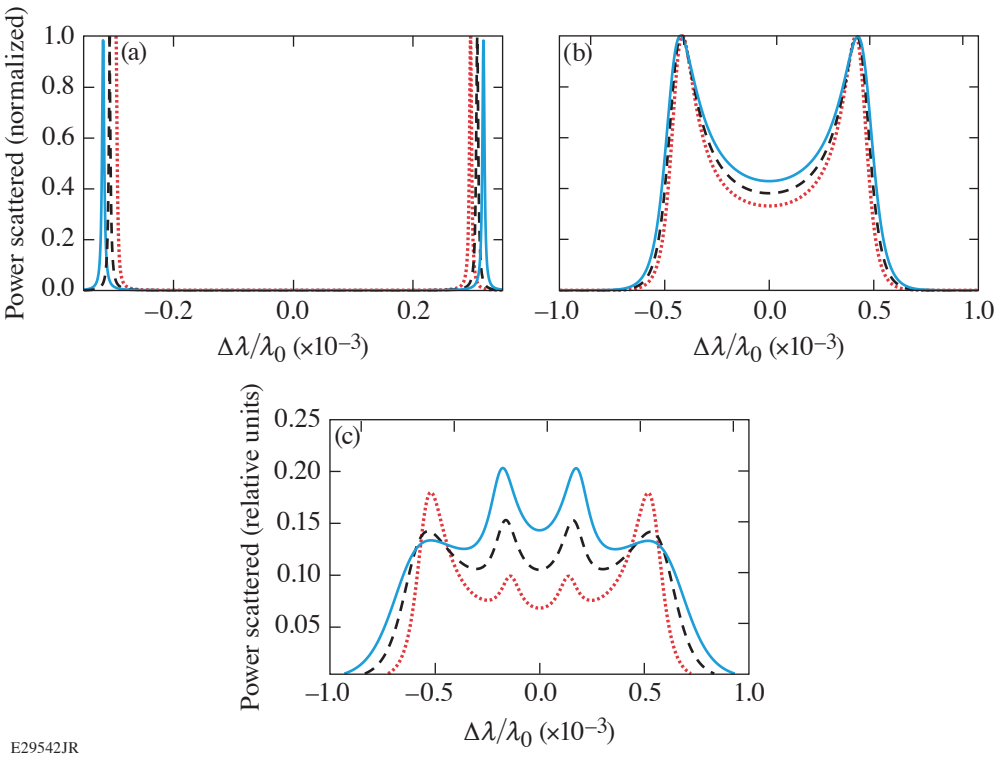

Figure 4

Low-frequency spectrum (a) for a single species nitrogen plasma, where ZT_e = 630 eV (red), ZT_e = 700 eV (black), and ZT_e = 770 eV (blue), where T_i = 20 eV. (b) In the mildly damped regime, the width of the ion feature can be used to measure the ion temperature: T_i = 18 eV (red), T_i = 20 eV (black), T_i = 22 eV (blue), and ZT_e = 700 eV. (c) Introducing 5% nitrogen (Z = 7) to a hydrogen (Z = 1) plasma provides two low-frequency modes, and their relative amplitudes provide an accurate measure of the ion temperature: T_e/T_i = 5 (red), T_e/T_i = 3.3 (black), T_e/T_i = 2.5 (blue); and T_e = 100 eV was held constant. For all calculations, α = 2.

This material is based upon work supported by the Department of Energy National Nuclear Security Administration under Award Number DE-NA0003856, the University of Rochester, and the New York State Energy Research and Development Authority. The support of DOE does not constitute an endorsement by DOE of the views expressed in this paper.

1. D. H. Froula *et al.*, *Plasma Scattering of Electromagnetic Radiation: Theory and Measurement Techniques*, 2nd ed. (Academic Press, Amsterdam, 2011).
2. A. L. Milder *et al.*, Phys. Rev. Lett. **124**, 025001 (2020).
3. A. Milder *et al.*, Phys. Rev. Lett. **127**, 015001 (2021).
4. A. Milder *et al.*, Phys. Plasmas **28**, 082102 (2021).
5. S. H. Glenzer *et al.*, Phys. Rev. Lett. **77**, 1496 (1996).
6. D. H. Froula *et al.*, Phys. Plasmas **9**, 4709 (2002).
7. J. S. Ross *et al.*, Rev. Sci. Instrum. **81**, 10D523 (2010).
8. D. H. Froula *et al.*, Rev. Sci. Instrum. **77**, 10E522 (2006).
9. A. M. Hansen *et al.*, Phys. Plasmas **26**, 103110 (2019.
10. T. J. Kessler *et al.*, Proc. SPIE **1870**, 95 (1993).
11. J. S. Ross *et al.*, J. Instrum. **6**, P08004 (2011).
12. J. Katz *et al.*, Rev. Sci. Instrum. **83**, 10E349 (2012).
13. A. Visco *et al.*, Rev. Sci. Instrum. **79**, 10F545 (2008).
14. J. Katz *et al.*, "A High Throughput, Pulse-Front-Tilt–Compensated Streaked Spectrometer for Picosecond Optical Thomson Scattering," presented at the 22nd Topical Conference on High Temperature Plasma Diagnostics, San Diego, CA, 16–19 April 2018.
15. A. S. Davies *et al.*, Phys. Rev. Lett. **122**, 155001 (2019).
16. R. K. Follett *et al.*, Rev. Sci. Instrum. **87**, 11E401 (2016).
17. E. A. Williams *et al.*, Phys. Plasmas **2**, 129 (1995).
18. D. H. Froula *et al.*, Phys. Plasmas **13**, 052704 (2006).